

1 **Human hippocampal theta oscillations reflect sequential dependencies during spatial**  
2 **planning.**

3  
4 Raphael Kaplan<sup>1,2</sup>, Adrià Tauste Campo<sup>3,4,5</sup>, Daniel Bush<sup>6,7</sup>, John King<sup>6,8</sup>, Alessandro  
5 Principe<sup>4</sup>, Raphael Koster<sup>1,6</sup>, Miguel Ley Nacher<sup>4</sup>, Rodrigo Rocamora<sup>4</sup>, & Karl J. Friston<sup>1</sup>

6  
7 1-Wellcome Centre for Human Neuroimaging, UCL Institute of Neurology, University  
8 College London, United Kingdom.

9 2-Kavli Institute for Systems Neuroscience, Norwegian University of Science and  
10 Technology, Trondheim, Norway

11 3-Center for Brain and Cognition, Department of Information and Communication  
12 Technologies, Universitat Pompeu Fabra, Barcelona, Spain

13 4-Epilepsy Unit, Department of Neurology, Hospital del Mar Medical Research Institute  
14 (IMIM), Barcelona, Spain.

15 5-Barcelonaβeta Brain Research Center, Pasqual Maragall Foundation, Barcelona, Spain.

16 6-UCL Institute of Cognitive Neuroscience, University College London, London, United  
17 Kingdom.

18 7-UCL Queen Square Institute of Neurology, University College London, London, United  
19 Kingdom.

20 8- Clinical, Education and Health Psychology, University College London, London, United  
21 Kingdom.

22 **Corresponding Author:** Raphael Kaplan; email: raphael.s.m.kaplan@ntnu.no, Kavli  
23 Institute for Systems Neuroscience, Norwegian University of Science and Technology Olav  
24 Kyrres gate 9, Trondheim, Norway 7030

25 **Keywords:** Hippocampus, Planning, Theta rhythm, Prospection, Sequential decision making,  
26 One-shot learning

27  
28

29 **Acknowledgements:** We thank Carmen Pérez Enríquez for helpful discussion and the staff at  
30 Hospital del Mar for help with patients. We would also like to thank David Bradbury and  
31 Letty Manyande for assistance with MEG experimental setup. We also thank the Wellcome  
32 Centre for Human Neuroimaging for providing facilities.

33

34 **Data Availability Statement:** The data that support the findings of this study are available on  
35 request from the corresponding author, RK. The data are not publicly available due to their  
36 containing information that could compromise the privacy of research participants.

37

38

39

40

41

42

43 **Abstract**

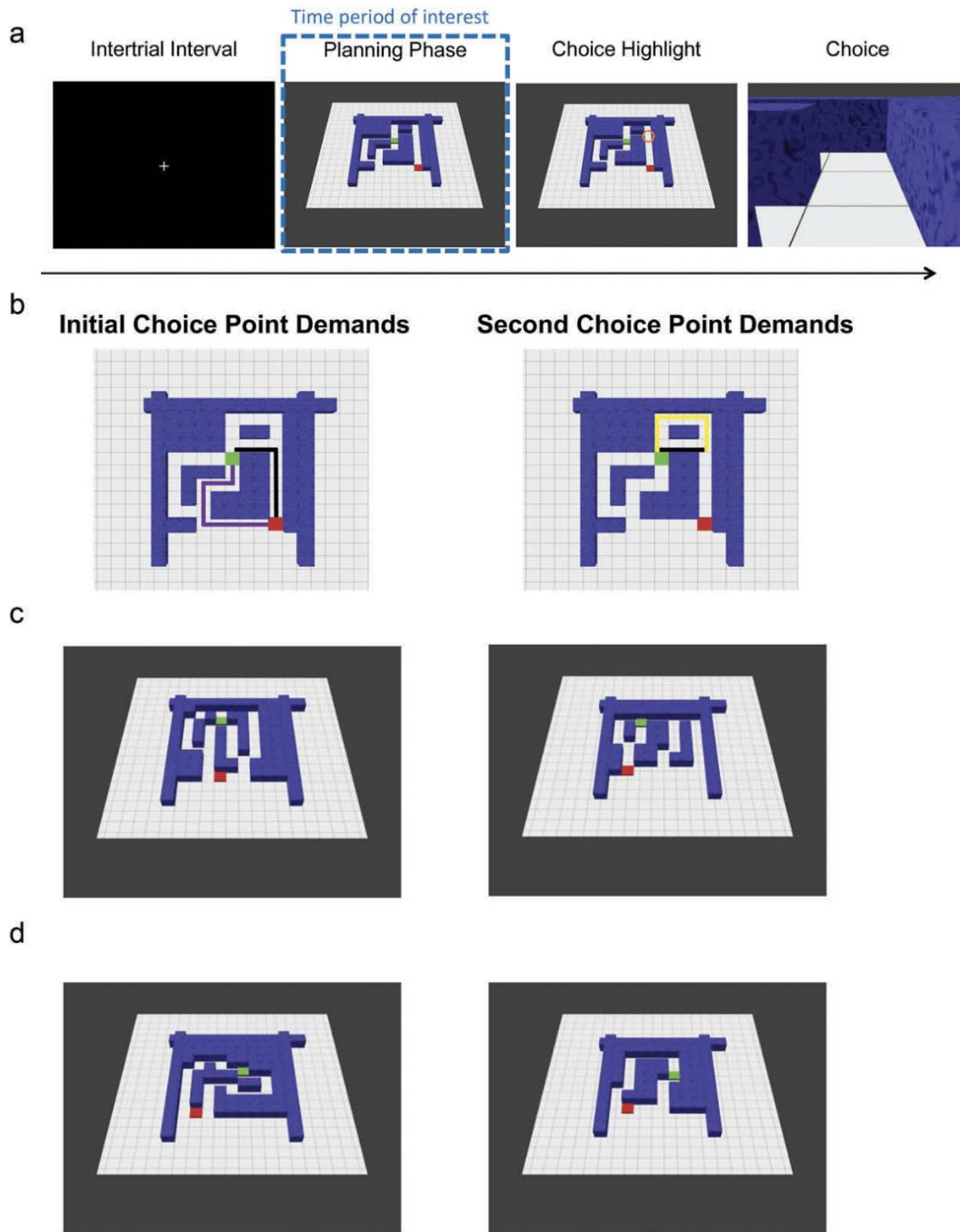
44 Movement-related theta oscillations in rodent hippocampus coordinate ‘forward sweeps’ of  
45 location-specific neural activity that could be used to evaluate spatial trajectories online. This  
46 raises the possibility that increases in human hippocampal theta power accompany the  
47 evaluation of upcoming spatial choices. To test this hypothesis, we measured neural  
48 oscillations during a spatial planning task that closely resembles a perceptual decision-making  
49 paradigm. In this task, participants searched visually for the shortest path between a start and  
50 goal location in novel mazes that contained multiple choice points, and were subsequently  
51 asked to make a spatial decision at one of those choice points. We observed ~4-8 Hz  
52 hippocampal/medial temporal lobe theta power increases specific to sequential planning that  
53 were negatively correlated with subsequent decision speed, where decision speed was  
54 inversely correlated with choice accuracy. These results implicate the hippocampal theta  
55 rhythm in decision tree search during planning in novel environments.

56

57 **Introduction**

58           Recent evidence has linked the hippocampus with planning in rodents (Miller et al.,  
59 2017) and humans (Kaplan et al., 2017a). Moreover, changes in hippocampal theta power  
60 (approx. 4-8Hz in humans) have been observed during memory-guided decision-making in  
61 well-learned environments in both species (Guitart-Masip et al., 2013; Schmidt et al., 2013;  
62 Belchior et al., 2014). However, it remains unclear whether changes in hippocampal theta  
63 power are associated with planning in novel environments. Notably, rodent type I  
64 hippocampal theta oscillations generated by exploratory movement (Vanderwolf, 1969) are  
65 linked to sweeps of place cell activity produced by hippocampal theta phase precession  
66 (O'Keefe & Recce, 1993). It has been hypothesized that these 'theta sweeps' could serve as a  
67 mechanism to plan trajectories online (Johnson & Redish, 2007). This raises the possibility  
68 that similar increases in human hippocampal theta power are induced by the planning of  
69 forward trajectories.

70           To investigate the role of the hippocampal theta rhythm in online spatial planning  
71 (i.e., the search of decision trees), we created a spatial task that required little to no learning,  
72 in which participants could draw upon their experience in the physical world (Kaplan et al.,  
73 2017a). We tested human participants on this task using non-invasive whole-head  
74 magnetoencephalography (MEG). Participants were instructed to visually search for the  
75 shortest path between a start and goal in novel mazes that afforded multiple paths.  
76 Participants were then asked which direction they would take from one of two choice points  
77 along the shortest path (Fig. 1).



78  
 79 **Fig 1. Task.** A. Each trial (i.e., visually presented maze) began with an inter-trial interval  
 80 (ITI) of 1.5s. Next, during a 3.25s planning phase, participants had to infer the shortest path  
 81 from a start point (red square) to a goal location (green square) and remember the chosen  
 82 direction for each choice point along the shortest path. A choice point was subsequently  
 83 highlighted (choice highlight) for 250ms. This was either the initial (i.e. first) or second (i.e.  
 84 subsequent) choice point along the shortest path. Participants were then asked which direction  
 85 (e.g., left or forward) they would take at that choice point during a choice period that was  
 86 cued by a first-person viewpoint of the highlighted location. Participants had a maximum of  
 87 1.5s to make their choice using a button box. B. Overhead view (not shown during the  
 88 experiment) of the maze in A, indicating which path lengths contribute to initial and second  
 89 choice point demands (black line represents shortest path). C. Left: Example sequential  
 90 planning trial with a small path length difference (demanding) at the red square/initial  
 91 choice point and large (less demanding) path length difference at the second choice point. Right:  
 92 Example trial with a large (less demanding) path length difference at the red square/initial

93 choice point and small (demanding) path length difference at the second choice point. D. Left:  
94 Example non-sequential (control) trial with a small path length difference (demanding).  
95 Right: Example non-sequential (control) trial with a large path length difference (less  
96 demanding).  
97

98           Crucially, the mazes were designed to induce forward planning in terms of a two-  
99 level tree search, where participants needed to maintain the decisions they made at each  
100 choice point. At both choice points, there was a small, medium, or large path length  
101 difference – creating a total of (3x3) nine conditions allowing us to test the effect of planning  
102 demands at each choice point depth (i.e., initial or second). In parallel, our task also contained  
103 a non-sequential control condition, where participants were presented with mazes containing  
104 only one choice point (Fig. 1D). In either case, we associate a smaller path difference with  
105 greater ambiguity and processing demands. Importantly, in any trial, participants were only  
106 prompted to make one choice after seeing the full maze; however, until the choice point was  
107 highlighted, they did not know which decision would be probed in sequential planning trials  
108 (Fig. 1). After planning their route, participants were asked to choose—at a specified choice  
109 point—the direction of the shortest path to the goal location (Fig. 1). This provided a measure  
110 (reaction time, RT) with which to quantify their (subjective) uncertainty to complement the  
111 (objective) difference in path lengths. This design allowed us to ask whether hippocampal  
112 theta power relates to successful sequential spatial planning.

113

## 114 **Methods**

### 115 *Participants*

#### 116 MEG

117           Twenty-four participants (14 female: mean age 23.5 yrs; SD of 3.49 years) gave  
118 written consent and were compensated for performing the experimental task, as approved by  
119 the local research ethics committee at University College London in accordance with  
120 Declaration of Helsinki protocols. All participants had normal or corrected-to-normal vision  
121 and reported to be in good health with no prior history of neurological disease. Due to

122 technical difficulties, two participants were removed from our sample, leaving twenty-two  
123 participants in the behavioral and MEG analyses presented here.

124 iEEG

125 Pre-surgical EEG recordings from 2 patients with pharmaco-resistant focal-onset  
126 seizures and hippocampal depth electrodes gave written consent, as approved by the local  
127 ethics committee at Hospital del Mar and in accordance with Declaration of Helsinki  
128 protocols. One patient was removed from analyses, because of visual difficulties due to an  
129 inferior occipital lesion, leaving one patient with normal vision presented in the current  
130 analysis. A summary of the patient's characteristics is given in Table 1.

131

132 *Experimental Design*

133 During MEG scanning, stimuli were presented via a digital LCD projector on a  
134 screen (height, 32 cm; width, 42 cm; distance from participant, ~70 cm) inside a magnetically  
135 shielded room using the Cogent (<http://www.vislab.ucl.ac.uk/cogent.php>) toolbox running in  
136 MATLAB (Mathworks, Natick, MA, USA). Instead of a projector, iEEG patients completed  
137 the task on a laptop in their hospital bed. There were no other differences with the MEG  
138 experiment unless mentioned otherwise. Over the course of 220 trials, participants viewed  
139 220 different mazes from a slightly tilted (overhead) viewpoint and later chose from first-  
140 person viewpoints within mazes generated using Blender (<http://www.blender.org>). All mazes  
141 had a starting location (a red square) towards the bottom of the maze and a goal location (a  
142 green square) further into the maze (Kaplan et al., 2017a). Mazes differed by hierarchical  
143 depth (number of paths to a goal location): there were 110 mazes with four possible routes  
144 (sequential mazes) and a further 110 non-sequential control mazes with two possible routes  
145 (control mazes). In the scanner, participants were first presented with pictures of novel mazes  
146 (Fig. 1) of varying difficulty (from an overhead viewpoint) and then asked to determine the  
147 shortest path from a starting location (a red square) at the bottom of the screen to the goal  
148 location (a green square). The overhead view appeared on the screen for 3.25 s, after which a  
149 location (choice point) along the path was highlighted briefly for 250 ms with an orange

150 circle. The choice point location could either be the initial choice point or a second  
151 (subsequent) choice point. Crucially, participants would only have to make a decision about  
152 one choice point for each trial.

153         At either choice point, it was necessary to choose between two possible directions,  
154 which could be left, forward, or right, with an additional option to select equal, if both routes  
155 were the same distance. The second choice point always fell on the optimal path from the  
156 starting location to the goal(Kaplan et al., 2017a). After the choice point was highlighted, a  
157 “zoomed in” viewpoint of this location (always one square back and facing the same direction  
158 as the overhead viewpoint) was presented. Participants had less than 1.5s (2s for the iEEG  
159 patient) to decide whether to go left, forward, right, or decide that all directions were  
160 equidistant to the goal. If no button press was made within the allotted duration, the trial  
161 counted as an incorrect trial and the experiment moved on to the 1.5s inter-trial interval (ITI)  
162 phase. Participants repeated this trial sequence 110 times per session, for a total of two  
163 sessions. Sessions lasted approximately 10–15 min.

164         All participants completed a brief practice session consisting of 40 mazes/trials before  
165 the experiment (on a laptop outside of the scanner). Sequential mazes contained two  
166 branch/choice points between routes further in the maze, and the path lengths from the initial  
167 choice point to either of the second choice points were always equal. In sequential mazes, we  
168 used a 3x3 factorial design. Path length differences were split between 2 (small difference), 4  
169 (medium difference), or 6 (large difference) squares (for an example, see square tiles in the  
170 mazes presented in Fig 1) for the two paths at the starting location and a path length  
171 difference of 2, 4, or 6 squares at the optimal choice point in the maze. There was one catch  
172 trial for sequential and control mazes in each session, each containing all equal path lengths  
173 (path length differences of 0). In sum, sequential maze trials could be 2, 2; 2, 4; 2, 6; 4, 2; 4,  
174 4; 4, 6; 6, 2; 6, 4; 6, 6; (e.g. 4, 2 would have a medium path length difference of 4 at the  
175 starting location, whereas the second choice point would have a small path length difference  
176 of 2). Half of the trials in the experiment were control/non-sequential mazes, which only

177 contained one choice point at the red starting square. For these mazes, path length differences  
178 were split between 2, 4, and 6, with one catch trial per session having equal path lengths.

179

#### 180 *iEEG recordings and artifact detection*

181 All iEEG recordings were performed using a standard clinical EEG system (XLTEK,  
182 subsidiary of Natus Medical, Pleasanton, CA) with a 500 Hz sampling rate. A unilateral  
183 implantation in the right hemisphere was performed accordingly, using 15 intracerebral  
184 electrodes (Dixi Médical, Besançon, France; diameter: 0.8 mm; 5 to 15 contacts, 2 mm long,  
185 1.5 mm apart) that were stereotactically inserted using robotic guidance (ROSA, Medtech  
186 Surgical, New York, NY).

187 Intracranial EEG signals were processed in a monopolar referencing montage because  
188 it has been found to be more sensitive than other montages in capturing hippocampal  
189 electrophysiological signals (Vila-Vidal et al., 2019). Still, it is important to note that  
190 monopolar referencing yields data that can be contaminated by volume conduction and  
191 remote field effects. All recordings were subjected to a zero phase, 400th order finite impulse  
192 response (FIR) band-pass filter to focus on our frequency range of interest (0.5-48 Hz) and  
193 remove the effect of alternating current. Audio triggers produced by the stimulus presentation  
194 laptop were recorded on the monitoring system, which allowed for the EEG to be aligned  
195 with trial onset information sampled at 25 Hz.

196 Although patients were consistently engaged by the task, all trials that included  
197 interictal spikes (IIS) or other artifacts, either within the period of interest or during the  
198 padding windows, were excluded from all analyses presented here after manual inspection (4  
199 trials removed). A 500 ms padding window was used at either end of planning period time  
200 series to minimize edge effects in subsequent analyses.

201

#### 202 *iEEG Time-Frequency Analysis*

203 Estimates of dynamic oscillatory power during periods of interest were obtained by  
204 convolving the EEG signal with a Morlet wavelet and squaring the absolute value of the



205 convolved signal. The wavelet transform was preferred to the Fourier transform here since the  
206 analysis was focused on preserving temporal information about when power changes  
207 happened, which is in contrast with MEG analyses that were more focused on source  
208 localization. To perform baseline correction on time–frequency data for display purposes,  
209 power values were averaged across ITI periods for each frequency band, and those average  
210 values were subtracted from the power values at each time point in the planning period. To  
211 assess correlations among oscillatory power in each trial with RT, oscillatory power at each  
212 time point and frequency of interest was correlated with trial-by-trial RTs. These values were  
213 then averaged across the deepest contacts in both anterior (x:34, y:-13, z:-23) and posterior  
214 (x:33, y:-31, z:-9) right hippocampal electrodes to provide a single value at each time and  
215 frequency point for the patient.

#### 216 *MEG recording and preprocessing*

217 Data were recorded continuously from 274 axial gradiometers using a CTF Omega  
218 whole-head system at a sampling rate of 600 Hz in third-order gradient configuration.  
219 Participants were also fitted with four electroculogram (EOG) electrodes to measure vertical  
220 and horizontal eye movements. MEG data analyses made use of custom made Matlab scripts,  
221 SPM8 &12 (Wellcome Centre for Human Neuroimaging, London; Litvak et al., 2011), and  
222 Fieldtrip (Oostenveld et al., 2011). For preprocessing, MEG data was epoched into 2s  
223 baseline periods prior to the planning phase for each of the nine sequential planning  
224 conditions of interest and the three non-sequential planning control conditions. Trials were  
225 visually inspected, with any trial featuring head movement or muscular artefacts being  
226 removed (mean trials removed per participant=3.45).

227

#### 228 *MEG Source Reconstruction*

229 The linearly constrained minimum variance (LCMV) scalar beamformer spatial filter  
230 algorithm was used to generate source activity maps in a 10-mm grid (Barnes et al., 2003).  
231 Coregistration to MNI coordinates was based on nasion, left and right preauricular fiducial

232 points. The forward model was derived from a single-shell model (Nolte, 2003) fit to the  
233 inner skull surface of the inverse normalized SPM template. The beamformer source  
234 reconstruction algorithm consists of two stages: first, based on the data covariance and lead  
235 field structure, weights are calculated which linearly map sensor data to each source location;  
236 and second, a summary statistic based on the mean oscillatory power between experimental  
237 conditions is calculated for each voxel. Focusing on the specifics of power estimation, sensor  
238 data have a Hann window applied and are then subject to a Fast Fourier transform (FFT) to  
239 estimate power at each frequency across the whole signal. FFT data from each sensor is then  
240 multiplied by the beamformer weights to estimate power in each source.

241 We wished to control for any possible influence of EOG muscular artefacts during the  
242 planning period on estimates of oscillatory power and therefore computed the variance of two  
243 simultaneously recorded EOG signals across each planning phase and removed any  
244 covariance between these EOG variance values and oscillatory power measurements across  
245 voxels by linear regression (Kaplan et al., 2014, 2017c). This left ‘residual’ oscillatory power  
246 measurements for all trials whose variance could not be accounted for by changes in the EOG  
247 signal between trials, and these residual values were used as summary images for subsequent  
248 analyses. RT was included as an additional nuisance regressor for the theta power source  
249 analysis investigating the effect of path length differences at different choice points. Including  
250 RT as a nuisance regressor specifically for this analysis helped determine whether there were  
251 any residual hippocampal theta power effects related to choice point demands during the  
252 planning period.

253

#### 254 *MEG Sensor-level Analyses*

255 For visualization purposes, scalp power plots were estimated by averaging Morlet  
256 wavelet transforms over the entire 3.25s planning period and 4-8Hz frequency window of  
257 interest. The sensor-level analysis followed the same EOG variance nuisance regression  
258 procedure as source analyses. Subsequently, the linear relationship between trial-by-trial RT

259 and residual 4-8Hz planning period oscillatory power values at each sensor was calculated for  
260 every participant.

261

### 262 *MEG Statistical Analyses*

263 There were two main periods of interest, the 1.5s ITI and 3.25s planning phase. For  
264 each of the 9 sequential planning regressors of interest (i.e., maze with a small, medium, or  
265 large path length at the second and initial points), we constructed parametric regressors based  
266 on RT and accuracy (i.e. whether the response was correct). Inferences about these effects  
267 were based upon t- and F-tests using the standard summary statistic approach for second level  
268 random effects analysis.

269 A peak voxel significance threshold of  $p < 0.05$  FWE corrected for multiple  
270 comparisons was used for MEG source analyses. Given the previously hypothesized role of  
271 the hippocampus theta rhythm in planning, we report whether peak-voxels in that frequency  
272 band and these regions survive small-volume correction for multiple comparisons ( $p < 0.05$ )  
273 based on a bilateral ROI of the hippocampus (mask created using Neurosynth, Yarkoni et al.,  
274 2011). All images are displayed at the  $p < 0.001$  uncorrected threshold for illustrative purposes.  
275 Additionally, only sources containing a significant peak voxel are displayed.

276 Post hoc statistical analyses were conducted using 10-mm radius spheres around the  
277 respective peak voxel specified in the GLM analysis. This allowed us to compare the effects  
278 of different regressors of interest, while ensuring we did not make any biased inferences in  
279 our post hoc analyses.

280

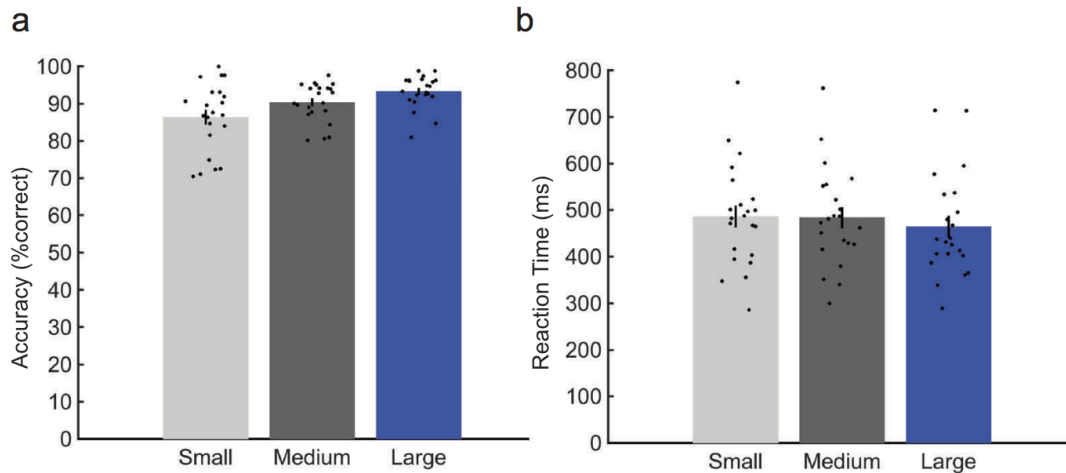
## 281 **Results**

### 282 *Behavioral Performance*

283 Twenty-two participants in the MEG study made correct choices on  $87.9 \pm 6.13\%$  of  
284 sequential planning trials (mean  $\pm$  SD; non-sequential control trials:  $86.4 \pm 4.95\%$ ), with an  
285 average reaction time (RT) of  $469 \pm 99$ ms (non-sequential control trials:  $363 \pm 112$ ms).  
286 Paired t-tests showed that RTs were significantly higher for sequential than non-sequential

287 (i.e. control) trials ( $t(21)=9.55$ ;  $p<.001$ ), without any difference in accuracy ( $t(21)=1.42$ ;  
288  $p=.171$ ). In addition, RTs were strongly inversely correlated with accuracy across MEG  
289 participants in both sequential ( $t(21)=-5.72$ ;  $p<0.001$ ) and non-sequential control trials  
290 ( $t(21)=-5.72$ ;  $p<.001$ ). After accounting for planning demands induced by the path length  
291 differences at each choice point (mean path length differences at the two choice points), RTs  
292 were still negatively correlated with accuracy in both sequential ( $t(21)=-5.25$ ;  $p<.001$ ) and  
293 non-sequential control trials ( $t(21)=-5.14$ ;  $p<.001$ ). In other words, participants responded  
294 faster when they made accurate choices. Moreover, these results demonstrate that RTs  
295 directly relate to accurate performance on the spatial planning task.

296 We then asked whether accuracy and RT were specifically influenced by path length  
297 differences and choice point depth, with the aim of disentangling the effects of first/initial  
298 versus second/subsequent choice point demands on planning accuracy and RT. Using a  
299 repeated measures ANOVA, we looked for an effect of path length difference and choice  
300 point depth on accuracy and RTs in MEG participants. We observed a main effect of path  
301 length difference on both accuracy ( $F(2,20)=9.09$ ;  $p=.002$ ; Fig. 2A) and RTs  
302 ( $F(2,20)=5.06$ ;  $p=.017$ ; Fig. 2B), driven by higher accuracy and faster RTs for larger path  
303 length differences; as well as a significant interaction between initial (i.e. first) and second  
304 (i.e. subsequent) choice points and path length differences on both accuracy ( $F(4,18)=11.0$ ;  
305  $p<0.001$ ) and RTs ( $F(4,18)=4.75$ ;  $p=0.009$ ). Post-hoc t-tests revealed that this interaction  
306 resulted from medium path length differences being significantly less demanding (i.e.  
307 producing higher accuracy and faster RTs) when they were at the initial, as opposed to the  
308 second, choice point (Accuracy:  $t(21)=3.62$ ;  $p=.002$ ; RT:  $t(21)=-4.17$ ;  $p<.001$ ).



309 **Figure 2: Behavior** A. Accuracy. Left: Significant main effect ( $p=0.002$ ) of path length  
 310 differences (small, medium, and large) on choice accuracy, collapsed across initial and second  
 311 choice points. B. Reaction time. Significant main effect ( $p=0.017$ ) of path length differences  
 312 (small, medium, and large) on reaction times, collapsed across initial and second choice  
 313 points. All error bars show  $\pm$  SEM.  
 314

315  
 316 *MEG Analyses*

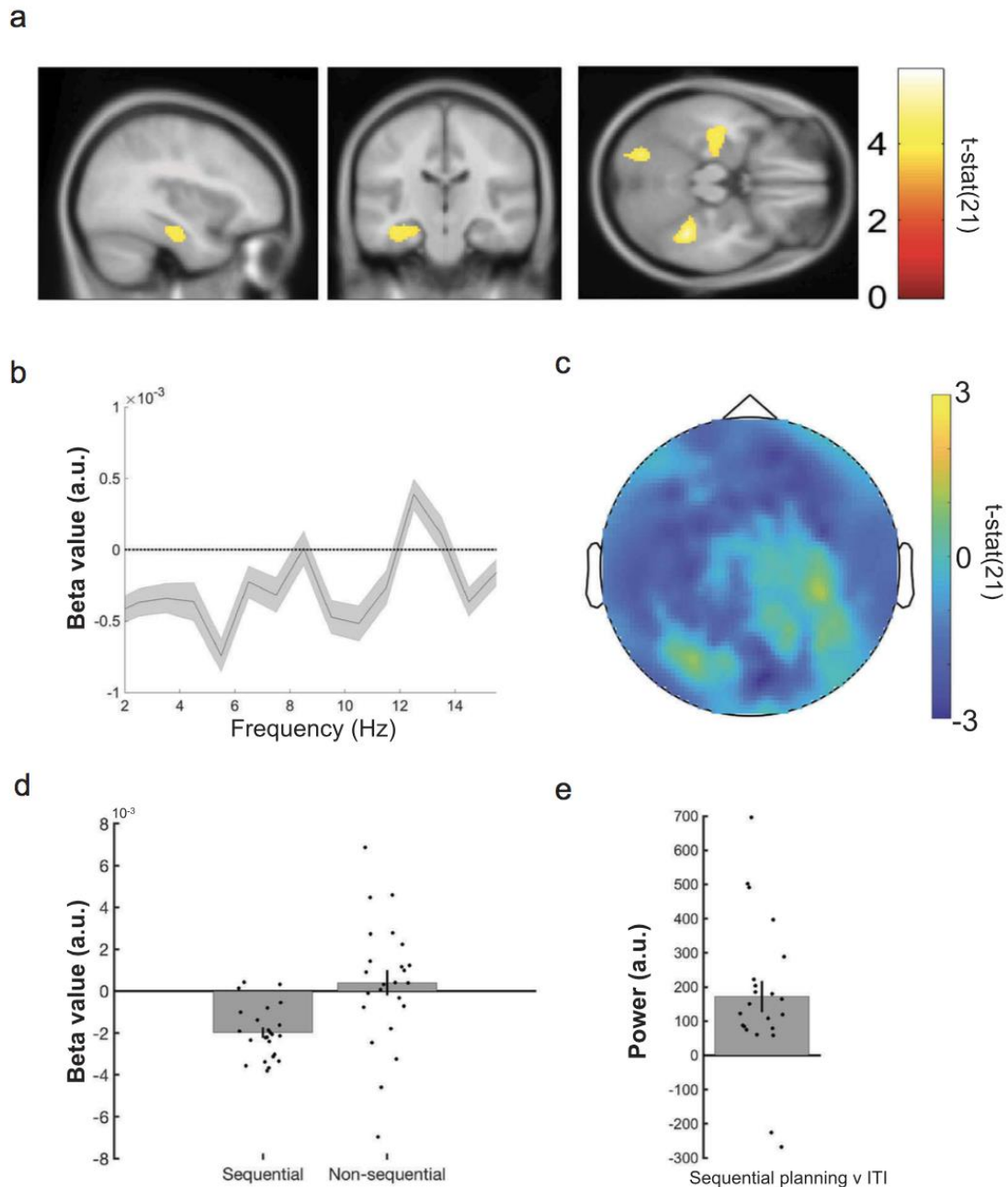
317 Using MEG source reconstruction, we asked whether 4-8 Hz theta power changes  
 318 anywhere in the brain were related to differences in spatial planning. As a control to ascertain  
 319 whether effects were specific to the theta frequency band, we also report power changes in  
 320 four other canonical frequency bands (delta / low theta: 1-3 Hz, alpha: 9-12Hz, beta: 13-  
 321 30Hz, and gamma: 30-80Hz). Focusing on RTs, we found a significant negative correlation  
 322 between 4-8Hz theta power during the sequential planning phase and subsequent RTs in a left  
 323 hippocampal source ( $x:-36, y:-20, z:-20, t(21)=-4.28$ ; small volume corrected (SVC) peak-  
 324 voxel  $p=.011$ ; Fig. 3A-B). Specifically, increased hippocampal theta power during planning  
 325 periods preceded faster decisions – an effect that was also visible at the scalp level (Fig. 3C).  
 326 Notably, we did not observe any correlation between theta power and trial-by-trial choice  
 327 accuracy anywhere in the brain, although this may be due to a relatively small number of  
 328 errors.

329 In addition, we found a significant negative correlation between theta power and RTs  
 330 in the right ventral temporal lobe ( $x:36, y:-42, z:-26; t(21)=-5.92$ ; family wise error (FWE)  
 331 corrected peak-voxel  $p=.012$ ; Fig. S1), which extended into posterior parahippocampal  
 332 cortex. We did not observe a significant positive correlation between 4-8Hz planning period

333 theta power and subsequent RTs anywhere in the brain. Elsewhere, we observed 9-12Hz  
334 alpha power changes in the right occipital lobe/cerebellum that negatively correlated with RT  
335 ( $x:28, y:-70, z:-22; t(21)=-5.99$ ; FWE corrected peak-voxel  $p=.014$ ; Fig. S1). However, we  
336 observed no other significant correlations between oscillatory power and RT in any other  
337 brain regions or frequency band.

338 To assess whether significant power changes related specifically to sequential  
339 planning, we tested whether each correlation described above was stronger for sequential  
340 planning trials versus non-sequential/control trials. Using a 10mm sphere around the  
341 respective peak voxels, we directly compared sequential versus non-sequential planning  
342 correlations with RT and observed that hippocampal RT theta effects selectively  
343 corresponded to sequential planning ( $t(21)=-2.33$ ;  $p=.03$ ; Fig. 3D). On the other hand, right  
344 ventral temporal/parahippocampal theta ( $t(21)=-1.38$ ;  $p=.181$ ; Fig. S1) and  
345 occipital/cerebellar alpha effects did not show any significant differences ( $t(21)=-1.74$ ;  
346  $p=.095$ ; Fig. S1). We did not observe any significant correlation between alpha or theta power  
347 and RT in any brain region during non-sequential control trials.

348 We then asked whether sequential spatial planning was associated with a general  
349 increase in left hippocampal theta power. Again, using a 10mm sphere around the left  
350 hippocampal peak, we observed a significant increase in 4-8Hz hippocampal theta power in  
351 this region during the sequential planning period versus ITI ( $t(21)=3.74$ ;  $p=.001$ ; Fig. 3E).  
352 Conducting the same sequential planning versus ITI analysis in the other areas exhibiting RT  
353 effects, we observed significant increases in both ventral temporal lobe theta ( $t(21)=2.79$ ;  
354  $p=.011$ ) and occipital alpha ( $t(21)=4.44$ ;  $p<.001$ ) power during sequential planning (Fig. S1).



355  
356  
357  
358  
359  
360  
361  
362  
363  
364  
365  
366  
367  
368  
369

**Fig. 3 Reaction time correlation with MEG theta power.**

A. Linearly Constrained Minimum Variance (LCMV) beamformer source reconstruction image showing significant 4-8 Hz left hippocampal theta power source negative correlation with RT ( $x:-36, y:-20, z:-20$ ) in 22 healthy participants. Images displayed at the statistical threshold of  $p < 0.001$  uncorrected for visualization purposes. B. Beta value spectrum from 1 to 15 Hz for hippocampal RT theta power effect showing peak negative correlation in the 4-8 Hz theta band. C. Negative 4-8 Hz theta power correlation with RT shown at the scalp level for 22 healthy participants. D. Data from a 10 mm sphere around left hippocampal peak voxel from RT contrast showing a significant difference ( $t(21) = -2.33; p = .03$ ) between sequential and non-sequential planning trials. E. Data from a 10 mm sphere around left hippocampal peak voxel from RT contrast showing increased theta power ( $t(21) = 3.74; p = .001$ ) during planning phase versus the ITI period. All error bars show  $\pm$  SEM.

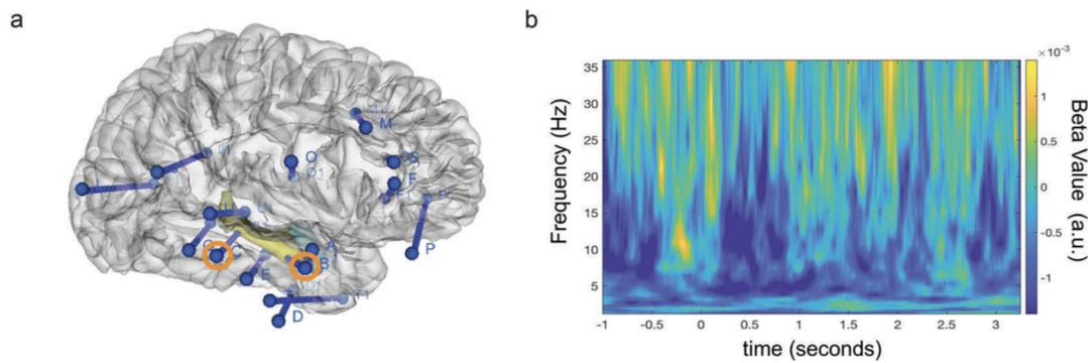
370 Finally, isolating hippocampal theta power changes, we tested for the effects of  
371 processing demands (path length differences) at initial and second choice points (e.g., quicker  
372 RT for mazes with less demanding initial choice points). Using a repeated measures ANOVA  
373 (path length difference by choice point depth), we tested whether the left hippocampal region  
374 (exhibiting a theta power correlation with RT) also showed an effect of path length  
375 differences at initial versus second choice points related to RT. We did not observe any  
376 significant effect of path length difference by choice point depth in the left hippocampus  
377 ( $F(4,18)=1.79$ ;  $p=.175$ ), or any other brain region.

378

### 379 *Hippocampal iEEG recordings*

380 Next, to corroborate our source reconstructed MEG effects, we examined changes in  
381 low frequency oscillatory power during the 3.25s sequential planning period using  
382 intracranial electroencephalography (iEEG) recordings from hippocampal depth electrodes  
383 (Fig. 4A) of a single high performing pre-surgical epilepsy patient (95.5% accuracy; mean  
384 RT:  $423 \pm 123$ ms). We asked whether iEEG 4-8Hz hippocampal theta power during  
385 sequential planning correlated with the patient's subsequent RT. Paralleling the MEG data  
386 described above, we observed a negative correlation between ~4-8 Hz hippocampal theta  
387 power during the entire 3.25s planning phase and subsequent RT ( $r=-0.202$ ;  $p=.035$ ; Fig. 4B).  
388 This result should be interpreted with caution given the relatively small number of  
389 measurements, the presence of an epileptic focus in the same hemisphere, lack of electrode  
390 coverage over adequate control regions, and presence of similar correlations at other  
391 frequencies. Overall, we observed hippocampal theta (along with alpha and beta) power  
392 correlations with RT during the sequential planning period that paralleled the theta effect we  
393 observed in the MEG dataset.





394

395 **Fig. 4 Intracranial EEG data from hippocampal depth electrodes** A. Image of electrode  
 396 locations in the patient overlaid on 3D brain template. Right hippocampal depth electrodes  
 397 with contacts used in the present analyses are highlighted in orange. B. Time-frequency plot  
 398 showing a negative correlation over trials between subsequent reaction time (RT) and 4-8 Hz  
 399 theta power during entire sequential planning period averaged across both hippocampal  
 400 contacts.

401

402

### General Discussion

403

404

405

406

407

408

409

We examined how the human hippocampal theta rhythm relates to planning sequential decisions in novel environments. Linking hippocampal theta to participants' performance on a spatial planning task, theta power during the planning phase correlated with faster subsequent spatial decisions. Furthermore, decision speed correlated with choice accuracy, regardless of path length differences. Linking the human hippocampal theta rhythm to processing demands, we found that hippocampal theta power selectively corresponded to planning performance in mazes containing multiple choice points during the MEG task.

410

411

412

413

414

415

416

417

418

419

Our observation of increased hippocampal theta power during spatial decision-making adds to an emerging literature investigating the role of the hippocampal theta rhythm during decision-making in rodents (Johnson & Redish, 2007; Schmidt et al., 2013; Belchior et al., 2014; Wikenheiser & Redish, 2015; Pezzulo et al., 2017) and humans (Guitart-Masip et al., 2013). Yet, the specific role of the hippocampal theta rhythm in planning has remained unclear; despite recent evidence relating the rodent (Miller et al., 2017) and human hippocampus (Kaplan et al., 2017a) to planning. Additional support for a hippocampal role in planning comes from evidence that hippocampal neurons code the distance to goal locations (Ekstrom et al., 2003; Villette et al., 2015; Sarel et al., 2017; Watrous et al., 2018). Furthermore, Wikenheiser and Redish (2015) found that firing of place cell sequences

420 coupled to the hippocampal theta rhythm extended further on journeys to distal goal locations.  
421 We parallel these findings by showing that hippocampal theta power was selectively related  
422 to efficient sequential planning.

423 Differing from previous MEG/iEEG hippocampal theta studies that observe power  
424 increases related generally to enhanced long- or short-term memory performance (Lega et al.,  
425 2012; Guitart-Masip et al., 2013; Olsen et al., 2013; Backus et al., 2016), we find  
426 hippocampal theta power effects associated with planning behavior in sequential, but not  
427 simpler mazes, during a task requiring little to no learning. Given the known relationship  
428 between the hippocampal theta rhythm and spatial trajectories, these findings may relate to  
429 sequential spatial decision-making that focuses on signifying a ‘location’ update within a  
430 sequence of choices. Supporting this explanation, recent work has suggested that the  
431 hippocampus can suppress noise in our everyday environment to focus on sub-goals during  
432 multi-step planning (Botvinick & Weinstein, 2014) and biophysical models predict that the  
433 hippocampal theta rhythm can underlie this type of ‘sub-goaling’ (Kaplan & Friston, 2018).

434 Still, several aspects of our results remain unclear. For instance, an alternative  
435 explanation for not observing right hemisphere or non-sequential hippocampal theta power  
436 spatial planning effects could be that there are multiple theta sources (e.g., anterior right vs  
437 posterior left hippocampus) corresponding to sequential and non-sequential RT effects (Miller  
438 et al., 2018), which MEG does not have adequate spatial resolution to resolve. Additionally,  
439 using eye movements as a nuisance regressor in our MEG data (and not measuring eye  
440 movements in our iEEG dataset) prevented us from examining the role of saccadic eye  
441 movements in this type of planning, which we have shown in a previous simulation to be a  
442 crucial component of our planning task (Kaplan & Friston, 2018). Despite finding  
443 hippocampal theta power selectivity to sequential planning, it is important to note that we  
444 didn’t observe any hypothesized change in theta power related to path length differences at  
445 the different choice points. One potential explanation for this null result is that hippocampal  
446 distance to goal coding is primarily related to single units, not oscillations (Ekstrom et al.,  
447 2003; Villette et al., 2015; Sarel et al., 2017; Watrous et al., 2018). Further evidence

448 supporting this explanation is needed since the direct relationship between behaviorally  
449 relevant hippocampal theta power changes and the reactivation of place cell sequences has yet  
450 to be characterized during sequential planning. Moving towards this characterization,  
451 Watrous and colleagues (2018) recently observed that human hippocampal single units  
452 exhibit phase-locking to the theta rhythm and that this phase-locking encoded information  
453 about goal locations during virtual navigation.

454 We studied multi-step planning in an explicitly spatial domain, but it isn't known  
455 whether updating our 'location' to subsequent choice points relates more to the overhead  
456 visual searches of the maze or a more abstract decision space (Kaplan et al., 2017b). On one  
457 hand, there is mounting evidence of the type I movement-related rodent hippocampal theta  
458 rhythm extending to virtual (Ekstrom et al., 2003, 2005; Watrous et al., 2011; Kaplan et al.,  
459 2012; Bush et al, 2017) and real-life navigation in humans (Aghajan et al., 2017; Bohbot et  
460 al., 2017). However, evidence from non-spatial domains is lacking. Future work exploring the  
461 role of the hippocampal theta rhythm in both perceptual exploration and abstract sequential  
462 decisions can determine how generalizable spatial planning-related hippocampal theta effects  
463 are to decision-making in other domains.

464

## 465 **References**

466

467 Aghajan Z, Schuette P, Fields TA, Tran ME, Siddiqui SM, Hasulak NR, Tchong TK, Eliashiv  
468 D, Mankin EA, Stern J, Fried I, Suthana N (2017) Theta Oscillations in the Human Medial  
469 Temporal Lobe during Real-World Ambulatory Movement. *Curr Biol*, 27:3743-51.

470

471 Backus AR, Schoffelen JM, Szebényi S, Hanslmayr S, Doeller CF (2016) Hippocampal-  
472 Prefrontal Theta Oscillations Support Memory Integration. *Curr Biol*, 26:450–7.

473

474 Barnes GR, Hillebrand A. Statistical flattening of MEG beamformer images (2003) *Hum*  
475 *Brain Mapp.* 18:1–12.

476

477 Belchior H, Lopes-Dos-Santos V, Tort AB, Ribeiro S (2014) Increase in hippocampal theta  
478 oscillations during spatial decision making. *Hippocampus*, 24:693-702.

479

480 Bohbot VD, Copara MS, Gotman J, Ekstrom AD (2017) Low-frequency theta oscillations in  
481 the human hippocampus during real-world and virtual navigation. *Nat Commun*, 8:14415.

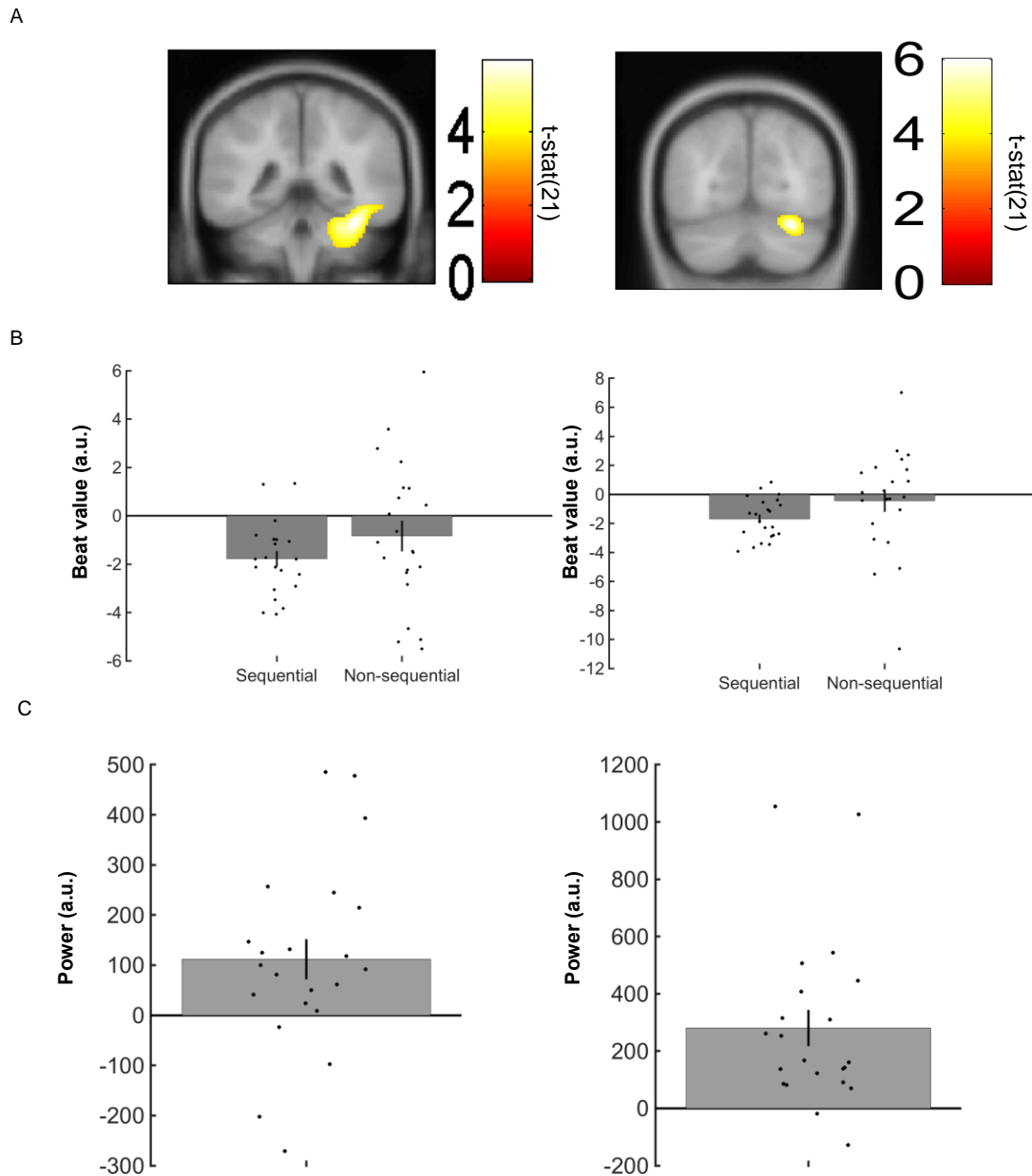
482

483 Botvinick M, Weinstein A (2014) Model-based hierarchical reinforcement learning and  
484 human action control. *Philos Trans R Soc Lond B Biol Sci*, 369

485

486 Bush D, Bisby JA, Bird CM, Gollwitzer S, Rodionov R, Diehl B, McEvoy AW, Walker MC,  
487 Burgess N (2017) Human hippocampal theta power indicates movement onset and distance  
488 travelled. *Proc Natl Acad Sci USA*, 114:12297-12302  
489  
490 Ekstrom AD, Kahana MJ, Caplan JB, Fields TA, Isham EA, Newman EL, Fried I (2003)  
491 Cellular networks underlying human spatial navigation. *Nature* 425:184-8  
492  
493 Ekstrom AD, Caplan JB, Ho E, Shattuck K, Fried I, Kahana MJ (2005) Human hippocampal  
494 theta activity during virtual navigation. *Hippocampus* 15:881-9  
495  
496 Fedorov A, Beichel R, Kalpathy-Cramer J, Finet J, Fillon-Robin J-C, Pujol S, Bauer C,  
497 Jennings D, Fennessy FM, Sonka M, Buatti J, Aylward SR, Miller JV, Pieper S, Kikinis R  
498 (2012) 3D Slicer as an Image Computing Platform for the Quantitative Imaging Network.  
499 *Magn Reson Imaging* 30:1323-41.  
500  
501 Guitart-Masip M, Barnes GR, Horner A, Bauer M, Dolan RJ, Duzel E (2013)  
502 Synchronization of medial temporal lobe and prefrontal rhythms in human decision making. *J*  
503 *Neurosci* 33:442-51.  
504  
505 Johnson A, Redish AD (2007) Neural ensembles in CA3 transiently encode paths forward of  
506 the animal at a decision point. *J Neurosci*, 27:12176-89.  
507  
508 Kaplan R, Doeller CF, Barnes GR, Litvak V, Düzel E, Bandettini PA, Burgess N (2012)  
509 Movement-related theta rhythm in humans: coordinating self-directed hippocampal learning.  
510 *PLoS Biol*, 10:e1001267.  
511  
512 Kaplan R, Bush D, Bonnefond M, Bandettini PA, Barnes GR, Doeller CF, Burgess N (2014)  
513 Medial prefrontal theta phase coupling during spatial memory retrieval. *Hippocampus*,  
514 24:656-65.  
515  
516 Kaplan R, King J, Koster R, Penny WD, Burgess N, Friston KJ (2017a) The Neural  
517 Representation of Prospective Choice during Spatial Planning and Decisions. *PLoS Biol*,  
518 15:e1002588.  
519  
520 Kaplan R, Schuck NW, Doeller CF (2017b) The Role of Mental Maps in Decision-Making.  
521 *Trends Neurosci*, 40:256-59.  
522  
523 Kaplan R, Bush D, Bisby JA, Horner AJ, Meyer SS, Burgess N (2017c) Medial Prefrontal-  
524 Medial Temporal Theta Phase Coupling in Dynamic Spatial Imagery. *J Cogn Neurosci*,  
525 29:507-19.  
526  
527 Kaplan R, Friston KJ (2018) Planning and navigation as active inference. *Biol Cybern*,  
528 112:323-43.  
529  
530 Lega BC, Jacobs J, Kahana MJ (2012) Human hippocampal theta oscillations and the  
531 formation of episodic memories. *Hippocampus*, 22:748-61.  
532  
533 Litvak V, Mattout J, Kiebel S, Phillips C, Henson R, Kilner J, Barnes G, Oostenveld R,  
534 Daunizeau J, Flandin G, Penny W, Friston K (2011) EEG and MEG data analysis in SPM8.  
535 *Comput Intell Neurosci.*, 2011:852961.  
536  
537 Miller J, Watrous AJ, Tsitsiklis M, Lee SA, Sheth SA, Schevon CA, Smith EH, Sperling MR,  
538 Sharan A, Asadi-Pooya AA, Worrell GA, Meisenhelter S, Inman CS, Davis KA, Lega B,  
539 Wanda PA, Das SR, Stein JM, Gorniak R, Jacobs J (2018) Lateralized hippocampal

540 oscillations underlie distinct aspects of human spatial memory and navigation. *Nat Commun*,  
541 9:2423.  
542  
543 Miller KJ, Botvinick MM, Brody CD (2017) Dorsal hippocampus contributes to model-  
544 planning. *Nat Neurosci*, 20:1269-76.  
545  
546 Nolte G (2003) The magnetic lead field theorem in the quasi-static approximation and its use  
547 for magnetoencephalography forward calculation in realistic volume conductor. *Phys Med  
548 Biol* 48:3637–3652.  
549  
550 O’Keefe J, Recce ML (1993) Phase relationship between hippocampal place units and the  
551 EEG theta rhythm. *Hippocampus*, 3:317-30.  
552  
553 Olsen RK, Rondina Ii R., Riggs L, Meltzer JA, Ryan JD (2013) Hippocampal and <sup>[1]</sup><sub>[SEP]</sub>  
554 neocortical oscillatory contributions to visuospatial binding and comparison. *Journal of  
555 Experimental Psychology: General* 142:1335-45. <sup>[1]</sup><sub>[SEP]</sub>  
556  
557 Oostenveld R, Fries P, Maris E, Schoffelen JM (2011) FieldTrip: Open source software for  
558 advanced analysis of MEG, EEG, and invasive electrophysiology data. *Comput Intell  
559 Neurosci*, 2011:156869.  
560  
561 Pezzulo G, Kemere C, van der Meer MAA (2017) Internally generated hippocampal  
562 sequences as a vantage point to probe future-oriented cognition. *Ann NY Acad Sci*, 1396:144-  
563 65.  
564  
565 Sarel A, Finkelstein A, Las L, Ulanovsky N (2017) Vectorial representation of spatial goals in  
566 the hippocampus of bats. *Science* 355:176-80  
567  
568 Schmidt B, Hinman JR, Jacobson TK, Szkudlarek E, Argraves M, Escabi MA, Markus EJ  
569 (2013) Dissociation between dorsal and ventral hippocampal theta oscillations during  
570 decision-making. *J Neurosci* 33:6212-24.  
571  
572 Vanderwolf CH (1969) Hippocampal electrical activity and voluntary movement in the rat.  
573 *Electroencephalogr Clin Neurophysiol*. 26:407-18.  
574  
575 Vila-Vidal M, Pérez Enriquez C, Principe A, Rocamora R, Deco G, Tauste Campo A (2019)  
576 Low entropy map of brain oscillatory activity identifies spatially localized events: a new  
577 method for automated epilepsy focus prediction. *bioRxiv*  
578  
579 Villette V, Malvache A, Tressard T, Dupuy N, Cossart R (2015) Internally Recurring  
580 Hippocampal Sequences as a Population Template of Spatiotemporal Information. *Neuron*,  
581 88:357-66.  
582  
583 Watrous AJ, Fried I, Ekstrom AD (2011) Behavioral correlates of human hippocampal delta  
584 and theta oscillations during navigation. *J Neurophysiol*, 105:1747-55.  
585  
586 Watrous AJ, Miller J, Qasim SE, Fried I, Jacobs J (2018) Phase-tuned neuronal firing encodes  
587 human contextual representations for navigational goals. *Elife*, 7  
588  
589 Wikenheiser AM, Redish AD (2015) Hippocampal theta sequences reflects current goals. *Nat  
590 Neurosci*, 18:289-94.  
591  
592 Yarkoni, T., Poldrack, R.A., Nichols, T.E., Van Essen, D.C., and Wager, T.D. (2011). Large-  
593 scale automated synthesis of human functional neuroimaging data. *Nat Methods*. 8, 665-70.  
594 **Supplemental Figure**



596

597

**Fig. S1 Additional reaction time correlations with MEG theta and alpha power**

598

A. Linearly Constrained Minimum Variance (LCMV) beamformer source reconstruction

599

images. Left: Shows significant 4-8 Hz right ventral temporal cortex theta power source

600

negative correlation with RT ( $x:36, y:-42, z:-26$ ) in 22 healthy participants. Right: Shows

601

significant 9-12 Hz right occipital/cerebellar cortex alpha power source negative correlation

602

with RT ( $x:28, y:-70, z:-22$ ). Images displayed at the threshold of  $p < 0.001$  uncorrected for

603

visualization purposes. B. Left: Data from a 10 mm sphere around right ventral temporal peak

604

voxel from RT contrast for both sequential and non-sequential/control planning trials. Right:

605

Data from a 10 mm sphere around right occipital peak voxel from RT contrast for both

606

sequential and non-sequential/control planning trials. C. Left: Data from a 10 mm sphere

607

around right ventral temporal peak voxel from RT contrast showing increased theta power

608

during planning phase versus the ITI period. Right: Data from a 10 mm sphere around right

609

occipital peak voxel from RT contrast showing increased theta power during planning phase

610

versus the ITI period. All error bars show  $\pm$  SEM.

611